Experimental study and numerical validation of oxy-ammonia combustion at elevated temperatures and pressures

Alka Karan, Guillaume Dayma, Christian Chauveau, Fabien Halter

Experimental study and numerical validation of oxy-ammonia combustion at elevated temperatures and pressures

A. Karan[a,b], G. Dayma[a,b], C. Chauveau[b], F. Halter[a,b]

[a] *Université d'Orléans, France*
[b] *CNRS-ICARE, Orléans, France*

Abstract

The combustion of fossil fuels, which are mostly based on hydrocarbon chains, produces large quantities of carbon dioxide which is a major contributor to the global warming. Due to alarming concerns, initiatives are taken to promote the use of 'zero-carbon fuel'. The use of ammonia as an alternative fuel in combustors like gas turbines and spark-ignition engines have already been tested. As high pressures and temperatures are encountered in these combustors, it is essential to find laminar flame speed data for ammonia combustion at these conditions. The present study focuses on performing experiments at elevated conditions for different equivalence ratios in a constant volume spherical chamber. A literature study was performed to select and evaluate the most recent kinetic mechanisms for ammonia combustion under these conditions. A sensitivity analysis highlighting the key reactions for two of the schemes has been performed. A range of exponential factors for temperature and pressure which is used to calculate the flame speeds for a given reference conditions : α and β have been determined.

Keywords: Ammonia, laminar flame speed, constant volume chamber, elevated conditions

1. Introduction

In the recent times, there is an extensive use of carbon-based fuels to meet with the ever-increasing demand for energy. This has resulted in a rapid depletion of fossil fuels along with an increase in carbon emissions and other green-house gases which is the primary cause of global warming

leading to climate change. Attempts are being made to curb the excessive usage of these conventional fuels by using alternative green fuels. Many countries have signed conventions like Kyoto protocol [1] and Paris agreement [2] which aim to reduce the emission of the green-house gases. Ammonia has received recent interests as it is carbon-free and relatively safe to store and transport. The use of ammonia as an alternative fuel in combustors like gas turbines [3] and especially in spark-ignition engines [4] has already been tested. Ammonia flames are characterized by a low combustion intensity, low laminar burning velocities and narrow flammability limits. Flame speed of ammonia in air at stoichiometry is as low as 7 cm/s at standard atmospheric conditions [5]. The low heating value (LHV) of ammonia is 18.8 MJ/kg which is lower than most of the commonly used fuels like hydrogen and methane [6]. Nevertheless, ammonia is favoured in spark-ignition engines as it has a high octane number. It has an energy density of 22.5 MJ/kg and can be stored in liquid form under 0.8 MPa at atmospheric temperature [7]. Ammonia is produced by the Haber-Bosch process which is the most economic way for mass production. This process can be made carbon-free to make it a green fuel. Hydrogen is obtained from the electrolysis of water with the help of solar and wind energy (renewable sources of energy) whereas nitrogen is obtained from air. Zamfirescu et al. [8] have shown that ammonia is the cheapest fuel per 100 km driving range and is cost-effective when compared to other fuels like hydrogen which also has an added disadvantage of risks in transportation. The flammability limits of ammonia (φ=0.63-1.4) compared to hydrogen (φ=0.1-7.1) [5] is quite low which makes it safer to store and transport but at the same time difficult to ignite making it an advantage and a disadvantage simultaneously. The economic statistics report by the ARPA-E, U.S. department of energy [9] show that ammonia is the most feasible form of energy delivery options for transportation when compared to both hydrogen and gasoline. The adiabatic flame temperature and the auto-ignition temperature of ammonia are at 1800°C and 650°C respectively making it a potential contender among other green fuels due to its anti-knock characteristics.

Despite the numerous properties which make ammonia a desirable fuel, there are a few added disadvantages in addition to the low flammability limit and the low LHV. It is known that ammonia is hazardous when released into the atmosphere due to its high toxicity. From the investigations made by Westlye et al. [10] on a spark-ignition engine, it was concluded that there may be unburned ammonia emissions along with intermediary oxides

of nitrogen which are harmful to the environment. To reduce the impact of these emissions, a selective catalytic reduction (SCR) was developed to promote complete combustion and also to ensure that the exhaust emissions do not pollute the environment.

The low speed of ammonia flames [11, 12] leads to an early blow-off and a difficulty in ignition. Ammonia is often combined with hydrogen or methane to increase the overall performance like the flame speeds, flammability limits and power output. Literature is available on different conditions for the combined fuel mixture [6, 13]. Data at high pressure and high temperature is available for ammonia mixed with hydrogen or methane [14, 15, 16, 17, 18]. However, for pure ammonia combustion, analyses have been made for a narrow range of pressure and temperature conditions for different equivalence ratios [12]. As high pressures and high temperatures conditions are encountered in spark-ignition engines and gas turbines, it is essential to find flame speed data for these conditions. The data available in the literature is attached as a supplementary document. It can be seen that the maximum flame speed for ammonia combustion is available for a pressure of 10 bar and a temperature of 473 K [18].

The present study focuses on performing experiments at high temperatures and pressures conditions for different equivalence ratios in a constant volume condition. The results of these experiments provide laminar flame speeds for a pressure range of 2 to 37 bar and a temperature range of 369 to 584 K at 3 different equivalence ratios (i.e. 0.8, 1.1 and 1.3). These results are further used to assess the most recent chemical kinetic schemes available in the literature at identical conditions. It is important to identify the key reactions and to ensure that the pressure and temperature dependence is well accounted for at elevated conditions.

2. Methodology

2.1. Experimental set-up

The accuracy of the measurement of the flame speeds is quite important as it affects the overall performances. Flame speed is a sizing parameter that influences the design of spark-ignition engines and gas turbines. The experiments were performed in the OPTIPRIME facility [19] of ICARE-CNRS, Orléans, France. One of the most common methods to measure the flame speeds is spherical flame propagating outwards in a constant volume chamber which has been deployed as the principal apparatus here. This method

allows making measurements at high initial temperatures and pressures [20]. The most interesting aspect of the set-up is that a 360° fused silica ring enables a full radial visibility. The flame front can be tracked from the ignition point which is at the centre of the spherical chamber to the walls where the flame propagates and finally extinguishes. The idea behind the vast visibility range is to be certain that the flame front remains spherical throughout the process without being influenced by gravity effects or instabilities and also to obtain the flame radius evolution over time. The apparatus also consists of a K-type thermocouple to measure the initial temperature and two pressure transducers (AVL GU21D) to measure the pressure simultaneously with the flame radius evolution from its ignition point.

2.2. Experiment conditions and measurement of flame speeds

The tests were performed for a mixture of ammonia-oxygen at 3 different equivalent ratios: 0.8, 1.1 and 1.3 at an initial temperature of 300 K. For the rich mixtures, the initial pressure ranged between 1 bar and 4 bar whereas for the lean mixture, it was at 1 bar and 2 bar. 30 % of the oxidiser mixture consists of oxygen and the remaining 70 % is the diluent for all the conditions. The diluent is required because these flames are quite unstable in nature as both hydrodynamic and thermo-diffusive instabilities are favoured in these temperature and pressure conditions. The Lewis number of ammonia flames is close to 1 and so, in order to increase the Lewis number, there is a need of adding bath gases with high thermal diffusivity. A combination of argon and helium was used to stabilise the flame. The ratio of the diluent was chosen such that the mixture could be readily ignited and the flame sustains till it hits the wall. It is difficult to ignite mixtures with a high helium content at low pressures as helium possesses a high thermal diffusivity. In the case of the high-pressure conditions, occurrence of instabilities is promoted and so, a large percentage of helium is required to stabilise the flame. The initial conditions used are represented in Table 1. The adiabatic flame temperature has been calculated and reported in Table 1. At this equilibrium condition, it is seen that the dissociation reaction of H_2O to OH is favoured.

Pressure was recorded during the experiment using the pressure transducers. The pressure in the chamber increases up to almost 10 times the initial pressure. Images were captured at the rate of 12000 fps using a CMOS camera (PHANTOM V1611) for all conditions. The images used to determine the flame speed spanned over the ignition point to the point where the flame front hits the wall. On using a code written in Matlab, the radius of the

Table 1: Initial conditions for the test cases along with the adiabatic flame temperature (AFT)

φ	$\mathbf{P_0}$ **(bar)**	**Diluent**	**AFT(K)**
0.8	1	49% Ar 21% He	2895
0.8	2	49% Ar 21% He	2944
1.1	1	49% Ar 21% He	2976
1.1	2	49% Ar 21% He	3036
1.1	1	21% Ar 49% He	2976
1.1	2	21% Ar 49% He	3036
1.1	3	21% Ar 49% He	3069
1.1	4	70% He	3093
1.3	1	49% Ar 21% He	2885
1.3	2	49% Ar 21% He	2927
1.3	2	21% Ar 49% He	2928
1.3	3	21% Ar 49% He	2950
1.3	4	21% Ar 49% He	2965
1.3	4	70% He	2965

flame at each frame was determined. The flame speed was calculated using the obtained radius and the corresponding pressure by the equation 1

$$S_u = \frac{dR_f}{dt} - \frac{(R_0^3 - R_f^3)}{3\gamma_u R_f^2 P}\frac{dP}{dt} \tag{1}$$

where R_f and R_0 represent the flame radius and the inner chamber radius respectively, P is the pressure in the chamber and γ_u is the heat capacity ratio of unburnt gas. Further details on this method can be found in [20, 21, 22, 23, 24].

2.3. Chemical Kinetics Schemes

Several numerical schemes are available in the literature. On performing a literature review [34, 35], it was understood that Okafor [30] gave the most congruent results for lean mixtures and Klippenstein [25] and Zhang [27] gave the best results for the fuel-rich mixtures. Konnov [36] and Mathieu [33] seem to over-estimate and under-estimate the flame speeds respectively when compared to the experimental data [5]. The most recent kinetic schemes were selected and are represented in Table 2. These mechanisms were used in the premixed laminar flame speed calculator available in Chemkin-Pro. The

Table 2: Chemical kinetic schemes used in this study

Kinetic Schemes	Species	Reactions	Reference
Klippenstein et al.	33	211	[25]
Dagaut et al.	42	250	[26]
Zhang et al. (2017)	37	229	[27]
Shrestha et al.	34	264	[28]
Nakamura et al.	38	232	[29]
Modified Okafor*	60	359	[30]
Otomo et al.	32	213	[31]
Stagni et al.	31	203	[32]
Mathieu and Petersen	55	278	[33]

* Okafor scheme was modified to add helium using the third body coefficients of argon.

flame speed was calculated for a pressure-temperature pair which evolved isotropically mimicking the experimental combustion process.

Among the 9 chosen mechanisms, it was seen that 2 mechanisms- Nakamura [29] and Stagni [32] predicted and captured the experimental results at all conditions better than the other mechanisms. Although, the 9 chosen mechanisms could aptly produce the trend, i.e. the flame speed increases with an isotropic increase of temperature and pressure for all the test conditions; there is a variation in the flame speed values. Sensitivity analyses were performed for a few mechanisms to understand the role of the key reactions.

3. Results and discussions

3.1. Experimental and numerical flame speeds

The experiments were performed in the isochoric condition. The isochoric method helps to retrieve a wide band of flame speed data at elevated conditions [20, 21, 22, 23, 24]. This range has been chosen such that the stretch effects that occur in the initial phase and the heat losses endured when the flame front hits the wall do not affect the propagation of the flame front and hence, the flame speed. Table 3 represents the range of pressure and temperature for which the flame speeds have been determined. It is assumed that the temperature of fresh gases evolves isentropically while the flame front propagates. A relative accuracy of less than 0.5% on the flame radius was propagated on the flame speed leading to a maximal error lower than 5% [20]. The experiment traces have been widened to account for this uncertainty.

Table 3: Initial pressure and equivalence ratio with the range of pressure and temperature for which the flame speed has been measured. The initial temperature, T_0, was maintained at 300K

φ	$\mathbf{P_0}$ **(bar)**	**P range (bar)**	**T range (K)**
0.8	1	2-6	369-502
0.8	2	4-16	374-555
1.1	1	2-9	371-572
1.1	2	4-16	371-557
1.1	3	6-30	372-584
1.1	4	8-37	371-575
1.3	1	2-8	370-544
1.3	2	4-17	370-555
1.3	3	6-26	370-557
1.3	4	8-36	369-563

The experimental flame speeds and the flame speeds from the chosen mechanisms were calculated and plotted for all the conditions given in Table 1. A very similar trend for all the given conditions was noted. However, most of the schemes failed to give the flame speed value within the experimental range. Generally, it was seen that the schemes of Klippenstein, Zhang (2017) and Dagaut over-estimate the flame speeds when compared to the experimental flame speed whereas Mathieu and Otomo under-estimate the flame speed. The other 4 mechanisms more or less fall within ± 5 % error bar of the experimental results. Out of the 14 cases, 3 of them are represented here in the Figures 1, 2 and 3. The 3 chosen conditions represent a fuel-lean condition, a fuel-rich condition and a high-pressure condition to illustrate the above mentioned observations. The chosen conditions help to demonstrate a fuel-rich versus fuel-lean mixture at similar initial conditions and a low pressure versus high pressure condition at the same equivalence ratio.

Figure 1 depicts the flame speed at φ=1.3, P_0=4 bar and T_0=302 K with a diluent mixture of 21% Ar and 49% He. Figure 2 represents the flame speed at φ=1.3, P_0=1 bar and T_0=296.8 K and Figure 3 represents the flame speed at φ=0.8, P_0=1 bar and T_0=296.2 K. Both the cases use the same diluent mixture: 49% Ar and 21% He. The flame speeds of the lean fuel-air ratio case, φ=0.8 is higher than that of the rich case, φ=1.3. The y axis represents the flame speed whereas the x axis is split as temperature and

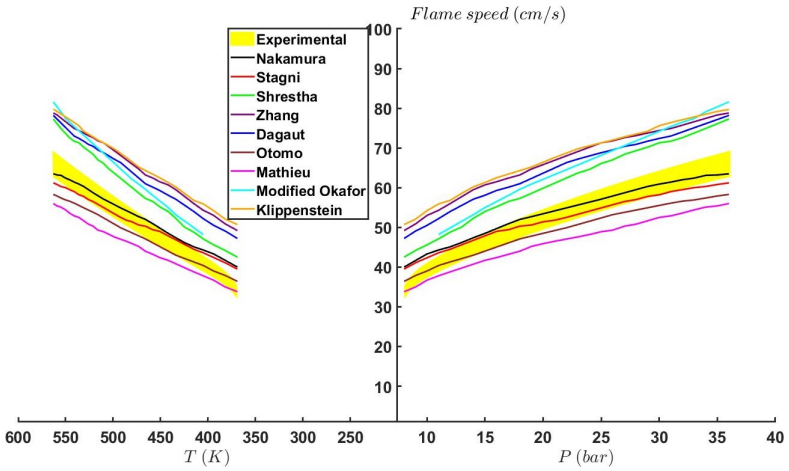

Figure 1: Laminar flame speeds at P_0=4 bar, T_0=302.3K, φ = 1.3, 21% Ar and 49% He.The experimental flame speeds have been thickened in yellow to account for the uncertainties incurred. The y axis represents the flame speed whereas the x axis is split as temperature and pressure. This is done as the flame speed is function of both pressure and temperature which evolves isotropically during the combustion process. The orange colour represents Klippenstein [25], violet represents Zhang (2017) [27], blue represents Dagaut [26], brown represents Otomo [31], pink represents Mathieu [33], cyan represents Modified Okafor [30], green represents Shrestha [28], red represents Stagni [32] and black represents Nakamura [29]

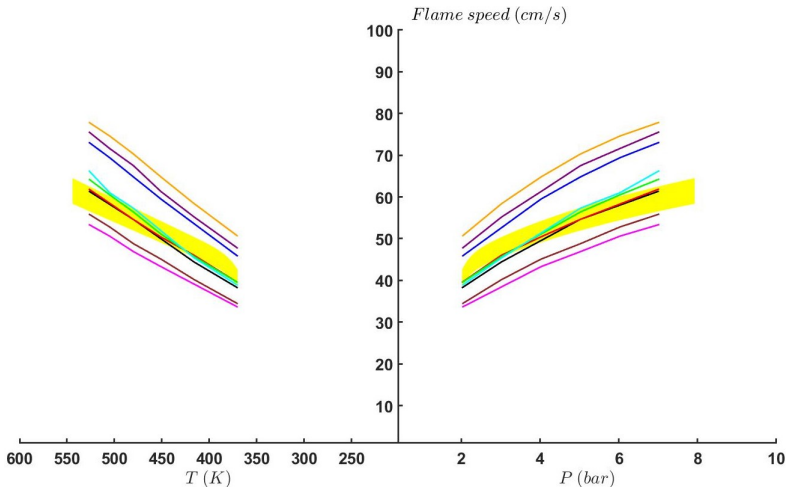

Figure 2: Laminar flame speeds at P_0=1 bar, T_0=296.8K, φ = 1.3, 49% Ar and 21% He

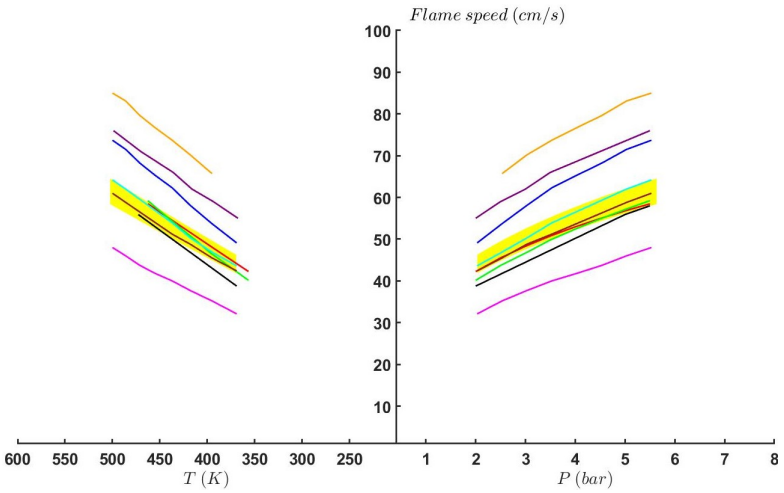

Figure 3: Laminar flame speeds at P_0=1 bar, T_0=296.2K, $\varphi = 0.8$, 49% Ar and 21% He

pressure. This is done as the flame speed is function of both pressure and temperature which evolves isotropically during the combustion process. On analysing all the cases, it was concluded that both Nakamura and Stagni can predict the flame speed closest to the experimental values. The experimental flame speeds along with the flame speeds from Nakamura and Stagni for all the cases are provided as supplementary document. Since, the study mainly focusses on 3 mechanisms, the following legend is maintained for convenience: red represents Stagni, black represents Nakamura and green represents Shrestha.

3.2. Sensitivity analyses

Sensitivity analyses were performed on a few mechanisms to understand the behaviour and to highlight the key reactions. It was seen that the most dominant reaction irrespective of the mechanism and the initial conditions is $O_2 + H \rightleftharpoons O + OH$. It is interesting to note that the sensitivity coefficient on the flow rate for the reactions for all the schemes are quite different even though the rate constant, k are quite similar. On comparing the rate constants of this reaction $O_2 + H \rightleftharpoons O + OH$ for Klippenstein and Nakamura and the flame speeds it can be confirmed that the discrepancy in the magnitude of flame speeds does not arise from the small difference in values of the k. The vast difference in the flame speeds for different mechanisms may be attributed to the global summation effect of those reactions that do not fall

under the top 10 important reactions. Since, Nakamura and Stagni estimate the flame speeds closer to the experimental results, a deeper study has been made on them.

Figures 4a, 4b and figures 5a, 5b depict the sensitivity analyses for Nakamura and Stagni mechanisms at $\varphi = 0.8$ and $\varphi = 1.1$ for an initial pressure of 1 bar and a diluent mixture of 49% Ar and 21% He respectively. Figures 6a, 6b represent the sensitivity analyses for Nakamura and Stagni mechanisms respectively at $\varphi = 1.1$, P_0=3 bar with a diluent mixture of 21% Ar and 49% He whereas figures 7a, 7b represent the analyses at $\varphi = 1.1$, P_0=4 bar and a diluent mixture of 70% He. Figures 8a, 8b and figures 9a, 9b display the sensitivity results at $\varphi = 1.3$ for a P_0=2 bar with a diluent mixture of 21% Ar and 49% He and for a P_0=4 bar with a diluent mixture of 70% He respectively. The analyses illustrate the use of different equivalence ratios, initial pressures and diluent mixtures. The sensitivity analyses for the remaining conditions are provided as a supplementary material. It is interesting to note that even though the flame speed predicted by Nakamura and Stagni are quite close, the top 10 important reactions are not exactly the same. The two common reactions apart from the dominant reaction are : $HNO + H \rightleftharpoons NO + H_2$ and $NH_2 + NO \rightleftharpoons NNH + OH$. It is noticed that the reaction $H_2 + O \rightleftharpoons H + OH$ exists within the top 10 important reactions in all cases for both the mechanisms except for the lean cases of Nakamura. The rich cases for both the mechanisms witnessed another 2 common reactions: $NH_2 + H \rightleftharpoons NH + H_2$ and $NH_2 + O \rightleftharpoons HNO + H$. A standard set of reactions is noted for each equivalence ratio apart from the above stated common reactions irrespective of the initial pressure except for $H + O_2 + (M) \rightleftharpoons HO_2 + (M)$ which is found only for those with an initial pressure of 2 bar or more. However, none of the stated reactions play a role as significant as the $O_2 + H \rightleftharpoons O + OH$ reaction does. Also, from the sensitivity analyses charts it can be seen that the flame speed is not highly sensitive to pressure. The sensitivity analyses show that these mechanisms predict a weak dependence of flame speed on pressure. On comparing with methane flames [20], the recombination reaction, $CH_3 + H \rightleftharpoons CH_4$ is one of the main reactions which becomes more sensitive at higher pressure and equivalence ratio. The equivalent recombination reaction in ammonia flames, $NH_2 + H \rightleftharpoons NH_3$ is not as sensitive as it is for the methane flames. Indeed, the mass burning rate is a parameter that indicates the reactivity. It increases as both the pressure and temperature increase for both ammonia and methane flames. It is known that when the pressure increases, the H radicals produced in the

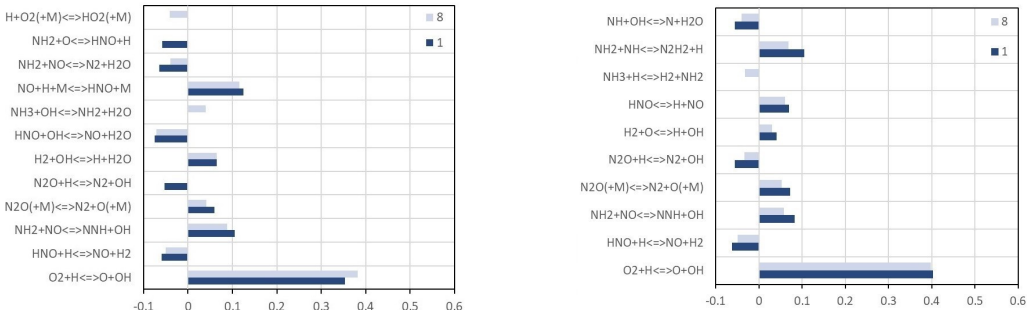

(a) Nakamura (b) Stagni

Figure 4: Sensitivity analyses at P_0=1 bar, $\varphi = 0.8$, 49% Ar and 21% He with the minimum pressure at 1 bar (dark blue) and the maximum at 8 bar (light blue)

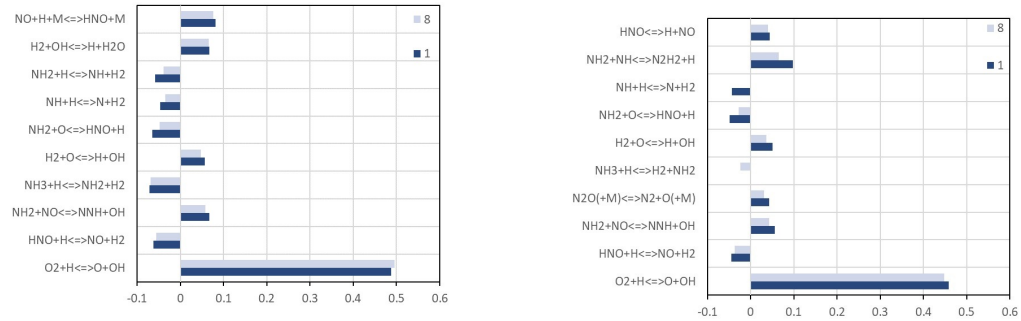

(a) Nakamura (b) Stagni

Figure 5: Sensitivity analyses at P_0=1 bar, $\varphi = 1.1$, 49% Ar and 21% He with the minimum pressure at 1 bar (dark blue) and the maximum at 8 bar (light blue)

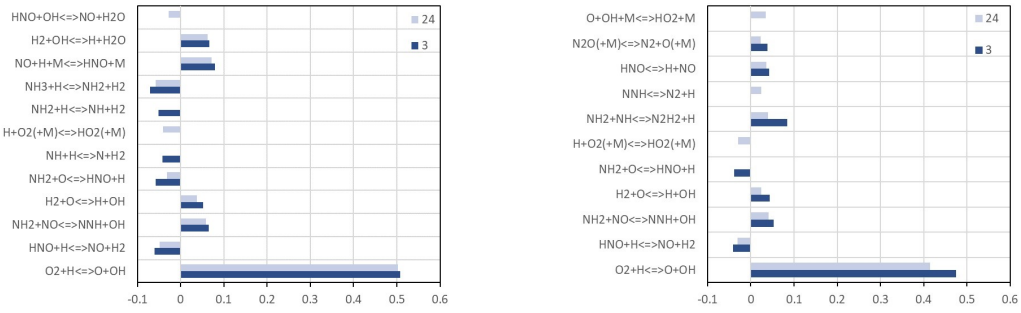

(a) Nakamura (b) Stagni

Figure 6: Sensitivity analyses at P_0=3 bar, $\varphi = 1.1$, 21% Ar and 49% He with the minimum pressure at 3 bar (dark blue) and the maximum at 24 bar (light blue)

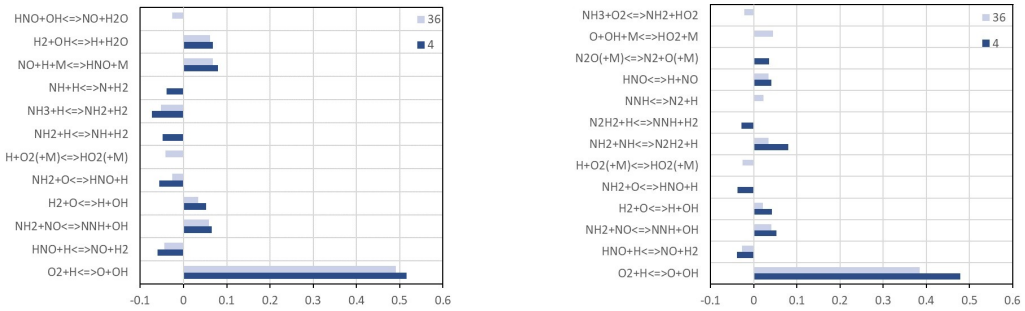

(a) Nakamura (b) Stagni

Figure 7: Sensitivity analyses at P_0=4 bar, $\varphi = 1.1$, 70% He with the minimum pressure at 4 bar (dark blue) and the maximum at 36 bar (light blue)

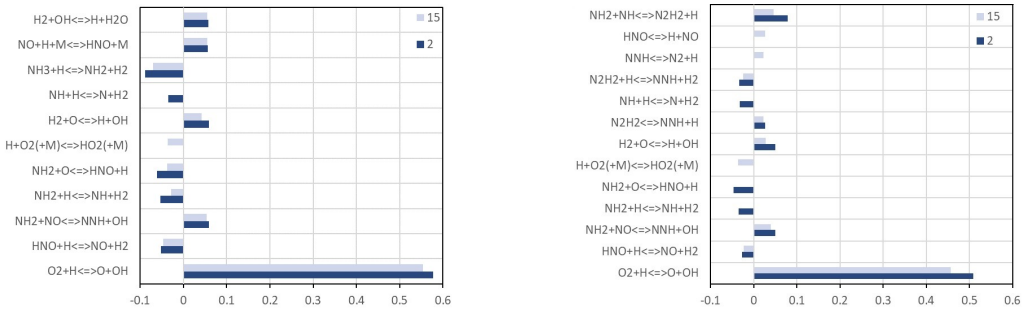

(a) Nakamura (b) Stagni

Figure 8: Sensitivity analyses at P_0=2 bar, $\varphi = 1.3$, 21% Ar and 49% He with the minimum pressure at 2 bar (dark blue) and the maximum at 15 bar (light blue)

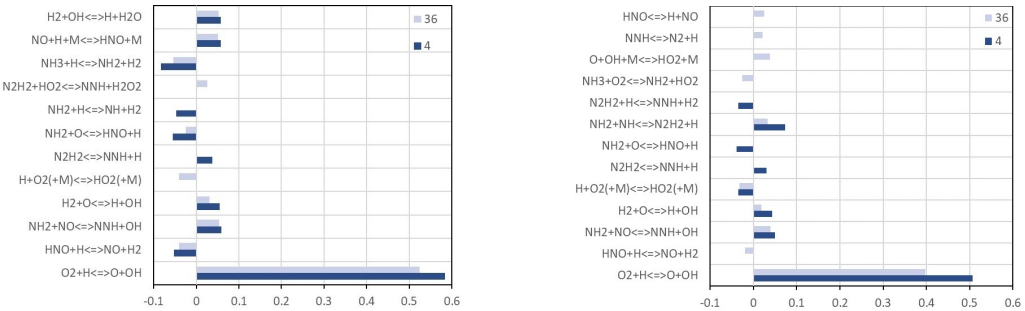

(a) Nakamura (b) Stagni

Figure 9: Sensitivity analyses at P_0=4 bar, $\varphi = 1.3$, 70% He with the minimum pressure at 4 bar (dark blue) and the maximum at 36 bar (light blue)

methane flames are more efficiently consumed leading to a decrease of flame speed. Here, to assess for ammonia flames, it may not be easy to conclude on the effect of the recombination reaction as the pressure and temperature increase simultaneously. To evaluate this effect, isothermal and isobaric sensitivity analyses have been carried out with one of the cases represented in the supplementary document. It is seen that $O_2 + H \rightleftharpoons O + OH$ is indeed the most sensitive reaction and the recombination reaction is not as sensitive as compared to the case of the methane flames. The dominance of the driving reaction whose rate constant is pressure-independent and the absence of the equivalent sensitive recombination reaction can possibly explain the ability of all the mechanisms to produce the experimental trend invariably.

Figures 1 and 2 represent the flame speed variation over pressure and temperature for a low-pressure and a high-pressure initial condition respectively. As shown in these figures, irrespective of a high-pressure and a low-pressure initial condition, it can be seen that the flame speed variation over a pressure difference of 30 and 6 bar are translated as a variation of about 180 K in the temperature scale. In other words, the flame speed change is much higher when the temperature changes by a small amount as compared to a variation in pressure. The temperature increase is higher at the beginning of the compression and this effect decreases at higher pressure. All of these suggest that the combustion of ammonia is more temperature-sensitive rather than being pressure-sensitive, thereby implying that the mechanisms may be temperature-driven and not pressure-driven. In order to understand the working of these mechanisms further study has been made.

3.3. Isotherms and isobars

Figure 10a depicts the variation of flame speed over pressure at T=300 K and Figure 10b over temperature at P=1 bar for 3 selected mechanisms: Nakamura, Stagni and Shrestha for $\varphi = 0.8$, 1.1 and 1.3 at a diluent mixture of 49% Ar and 21% He. Isotherms were plotted at T=300 K and at T=500 K and isobars were plotted for P=1 bar and P=3 bar. Similar results were obtained for both conditions. Isotherms at T=500 K and isobars at P=3 bar are provided as supplementary data. It is important to note that the flame speed axis range for the isobars are 4 times the range of the isotherms. It can be seen that as the pressure increases, the flame speed does not vary much. The drastic change in the flame speed is between 1-5 bar for all the mechanisms. As for the case of flame speed variation over the temperature, it is seen that the flame speed increases with temperature and the change

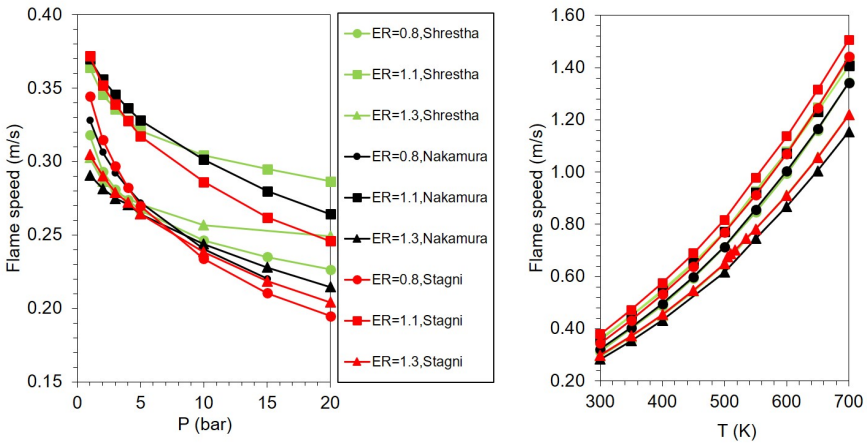

(a) Isothermal plots at T=300 K (b) Isobaric plots at P=1 bar

Figure 10: Comparison study of Nakamura, Stagni and Shrestha for $\varphi = 0.8$, 1.1 and 1.3 at a diluent mixture of 49% Ar and 21% He, circles represent $\varphi = 0.8$, squares represent $\varphi = 1.1$ and triangles represent $\varphi = 1.3$ whereas the colours green, black and red represent the mechanisms of Shrestha, Nakamura and Stagni respectively.

is prominent at higher temperature. This essentially proves that the mechanisms are indeed driven by temperature. On evaluating the performance of the 3 mechanisms, it can be said that the temperature effect is the same in the 3 mechanisms. Figure 10a suggests that the pressure effect is slightly more important in Stagni when compared to the other 2 mechanisms and the least in Shrestha.

The effect of the bath gases is studied and is displayed in figures 11a and 11b. Isotherms at T=300 K and 500 K and isobars at P=1 bar and 3 bar gave similar results. Isothermal plots at T=500 K are displayed in Figure 11a and isobaric plots at P=3 bar are shown in Figure 11b. The isotherms at T=300 K and isobars at P=1 bar are provided as supplementary data. It may be concluded that for the Shrestha mechanism the variation of the flame speed with pressure is independent of the bath gas composition while both Nakamura and Stagni show a slight dependence.

The pressure and temperature dependencies may be expressed as given in the equation 2 using a reference flame speed and the corresponding conditions if the exponential factors α and β are known.

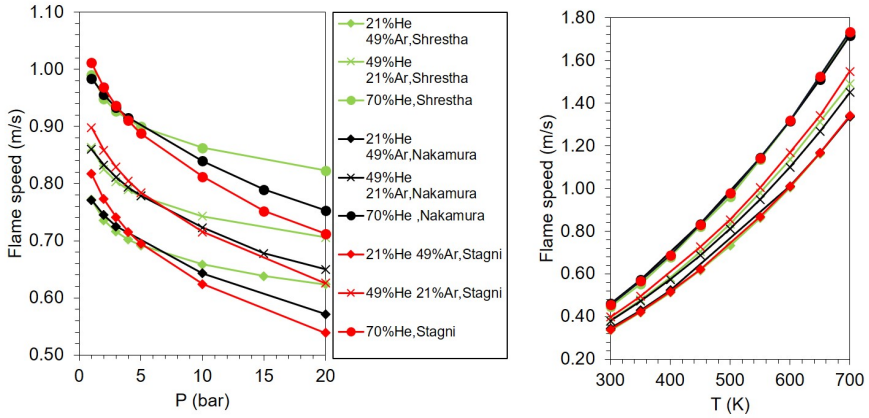

(a) Isothermal plots at T=500 K (b) Isobaric plots at P=3 bar

Figure 11: Comparison study of Nakamura, Stagni and Shrestha for $\varphi = 1.1$ for different bath gases compositions, circles represent 70% He, crosses represent 49% He and 21% Ar and diamonds represent 21% He and 49% Ar whereas the colours green, black and red represent the mechanisms of Shrestha, Nakamura and Stagni respectively.

$$\frac{S_u}{S_u^o} = (\frac{T_u}{T_u^o})^{\alpha}(\frac{P_u}{P_u^o})^{\beta} \tag{2}$$

Using the isothermal and isobaric curves, the values for α and β are estimated. It is observed that α varies linearly with the temperature for all the 3 mechanisms and the value ranges between 1.5 and 2. This range of value is quite common to most of the fuels [37]. β variation for Nakamura and Stagni is quadratic whereas it is almost a constant for Shrestha as seen in the Figure 12. Beta trends represented in the Figure 12 is calculated using P_0=1 bar, T_0= 500 K and the corresponding flame speed depending on the equivalence ratio and the diluent mixture. The values of β lies between -0.04 and -0.17 which is much lower than most of the fuels [37]. The low value of beta results from the pressure independent behaviour. It is worth emphasising that the pressure in-dependency increases with an increase in pressure.

3.4. Alpha and beta values for the experiment and numerical flame speeds

From the experimental test conditions, it is possible to have at least two conditions with the same equivalence ratio, initial temperature and diluent

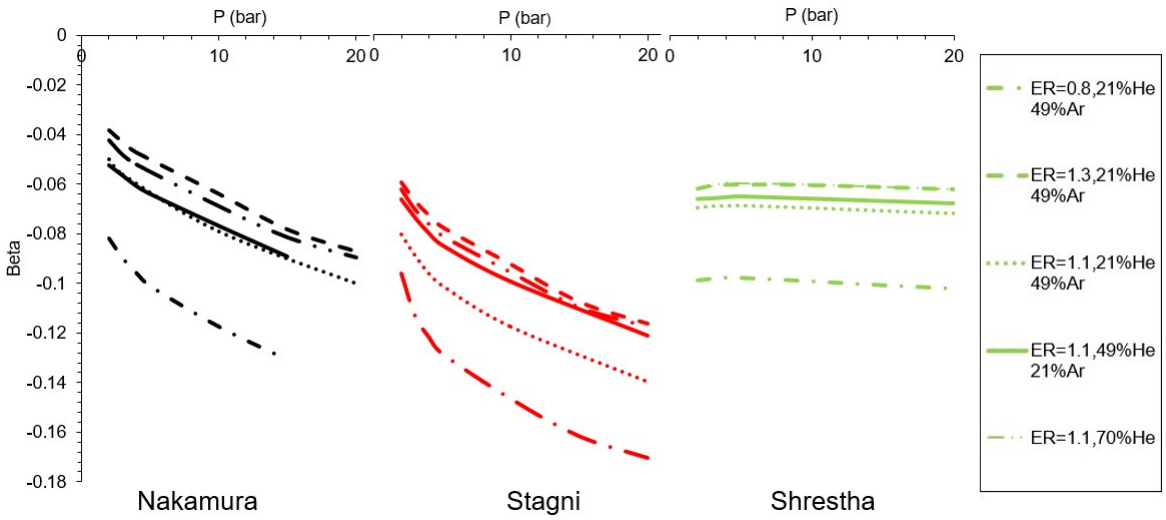

Figure 12: Beta trends from isotherms at T=500 K calculated using P_0=1 bar, T_0= 500 K and the corresponding flame speed depending on the equivalence ratio and the diluent mixture. φ=0.8, 21% He 49% Ar is represented by dash dot, φ=1.3, 21% He 49% Ar by dash, φ=1.1, 21% He 49% Ar by round dot, φ=1.1, 49% He 21% Ar by solid and φ=1.1, 70% He by long dash dot dot and the colours black, red and green represent Nakamura, Stagni and Shrestha respectively.

mixture but with a different initial pressure giving rise to two (P,T) pairs. A certain range of pressure is common to both the conditions but the corresponding temperatures are different due to the initial conditions. The flame speeds can be obtained for two different temperatures at an isobaric condition. Considering one of the flame speed curves (here, the flame speed corresponding to the initial condition with the lower pressure) as the reference curve, an estimation of α can be made using equation 2 and can be optimised to get the most precise value. A similar process can be used to estimate the β values from flame speeds corresponding to two different pressures at isothermal conditions.

The values of α and β from Nakamura and Stagni lies within the experiment range. The values of β ranges between -0.07 to -0.21 and the values of α range between 1.5 and 1.92 depending on the initial conditions. Both α and β are not constant values, therefore an estimation of the flame speed using equation 2 can be made by interpolating the values within the given range for the given set of conditions. It can be intuitively said that having a low β value is advantageous as pressure oscillations would have fewer effects on the flame stabilization in systems like gas turbines.

4. Conclusion

Experiments to measure flame speeds corresponding to the conditions encountered in spark-ignition engines and gas turbines have been performed. The study was done for 3 different equivalence ratios: 0.8, 1.1 and 1.3 at an initial temperature of 300 K and an initial pressure ranging from 1 to 4 bar. The data available in the literature gives the flame speeds for a maximum pressure of 10 bar and a temperature of 473 K. From this study, the laminar flame speeds for a pressure of 37 bar and a temperature of 584 K have been obtained. These tests were performed in constant volume condition which is the most efficient way to obtain a wide range of data for elevated conditions.

A literature study had been made to select the most recent kinetic schemes for ammonia combustion. These schemes have been evaluated for the same conditions as that of the experiments. It was seen that the chosen schemes could produce the experimental trend- increase of flame speed with an isotropic increase of pressure and temperature for all the conditions. On performing a sensitivity analyses, it was understood that the most dominant reaction is $O_2 + H \rightleftharpoons O + OH$. Despite the high sensitivity of this reaction and the rate constant of this reaction being similar for all mechanisms, only 4

mechanisms: Shrestha, Nakamura, Modified Okafor and Stagni could predict the flame speeds with the ± 5 % error bar of the experimental flame speeds. The recombination reaction of the ammonia flames is pressure insensitive. In order to understand the working of the mechanisms, various simulations were performed at isobaric and isothermal conditions. The results of these simulations prove that the mechanisms are temperature-driven and not pressure-driven as the change in flame speed for a small increase in temperature is much higher than the change in flame speed obtained from the same increase in pressure. The maximum influence of pressure is seen only from 1-5 bar after which the flame speeds do not vary a lot. The increase in the flame speed is attributed only to the increase of temperature which promotes the chemical reactivity. The impact of adding the bath gases has been noted for some of the mechanisms. The change in the flame speed response to pressure for Shrestha seems to have a lesser effect from the bath gases composition whereas Stagni and Nakamura seem to be influenced by the constituents of the bath gases.

A range of exponential factors α and β required to calculate the flame speeds at a given pressure and temperature using a reference condition was determined. It is interesting to note that β, the exponential factor for the pressure is much smaller than most of the fuels emphasising the pressure in-dependency behaviour. This implies that ammonia is an ideal fuel for spark-ignition engines and gas turbines since pressure oscillations would have limited effects on the flame speed.

It can be concluded that the performance of oxy-ammonia flames is in par with the conventional fuels and has a promising future. Ammonia being a non-carbon based fuel, indeed has the potential to replace the hydrocarbon fuels without a large compromise in performance.

5. Acknowledgements

We are thankful to the Université d'Orléans, Région Centre-Val de Loire and CNRS.

References

[1] The Kyoto Protocol in a Global Perspective, https://www.researchgate.net/publication/228373949_The_Kyoto_protocol _in_a_global_perspective.

[2] Paris Agreement, https://www.researchgate.net/publication/332524888_Paris_Agreement.

[3] A. Valera-Medina, D. Pugh, P. Marsh, G. Bulat, P. Bowen, Preliminary study on lean premixed combustion of ammonia-hydrogen for swirling gas turbine combustors, Int. J. Hydrog. Energy 42 (2017) 24495–24503.

[4] S. Frigo, R. Gentili, Analysis of the behaviour of a 4-stroke SI engine fuelled with ammonia and hydrogen, Int. J. Hydrog. Energy 38 (2013) 1607–1615.

[5] H. Kobayashi, A. Hayakawa, K. K. A. Somarathne, E. C. Okafor, Science and technology of ammonia combustion, Proc. Combust. Inst. 37 (2019) 109–133.

[6] C. Lhuillier, P. Brequigny, F. Contino, C. Mounaïm-Rousselle, Experimental study on NH_3/H_2/air combustion in spark-ignition engine conditions, 11^{th} Mediterranean Combustion Symposium (2019).

[7] A. Valera-Medina, H. Xiao, M. Owen-Jones, W. David, P. Bowen, Ammonia for power, Prog. Energy Combust. Sci. 69 (2018) 63–102.

[8] C. Zamfirescu, I. Dincer, Ammonia as a green fuel and hydrogen source for vehicular applications, Fuel Process. Technol. 90 (2009) 729–737.

[9] Advanced research projects agency-energy (ARPAE), U.S. Department of Energy, Renewable energy to fuels through utilization of energy-dense liquids (Refuel) (2016).

[10] F. R. Westlye, A. Ivarsson, J. Schramm, Experimental investigation of nitrogen based emissions from an ammonia fueled SI-engine, Fuel 111 (2013) 239–247.

[11] X. Han, Z. Wang, M. Costa, Z. Sun, Y. He, K. Cen, Experimental and kinetic modeling study of laminar burning velocities of NH_3/air, NH_3/H_2/air, NH_3/CO/air and NH_3/CH_4/air premixed flames, Combust. Flame 206 (2019) 214–226.

[12] A. Hayakawa, T. Goto, R. Mimoto, Y. Arakawa, T. Kudo, H. Kobayashi, Laminar burning velocity and markstein length of ammonia/air premixed flames at various pressures, Fuel 159 (2015) 98–106.

[13] C. Mørch, A. Bjerre, M. Gøttrup, S. Sorenson, J. Schramm, Ammonia/hydrogen mixtures in an SI-engine: Engine performance and analysis of a proposed fuel system, Fuel 90 (2011) 854–864.

[14] C. Duynslaegher, H. Jeanmart, J. Vandooren, Ammonia combustion at elevated pressure and temperature conditions, Fuel 89 (2010) 3540–3545.

[15] A. Goldmann, F. Dinkelacker, Approximation of laminar flame characteristics on premixed ammonia/hydrogen/nitrogen/air mixtures at elevated temperatures and pressures, Fuel 224 (2018) 366–378.

[16] C. Lhuillier, P. Brequigny, N. Lamoureux, F. Contino, C. Mounaïm-Rousselle, Experimental investigation on laminar burning velocities of ammonia/hydrogen/air mixtures at elevated temperatures, Fuel 263 (2020) 116653.

[17] J. Li, H. Huang, N. Kobayashi, Z. He, Y. Nagai, Study on using hydrogen and ammonia as fuels: Combustion characteristics and NO_x formation: Hydrogen and ammonia as fuels, Int. J. Energy Res. 38 (2014) 1214–1223.

[18] K. P. Shrestha, C. Lhuillier, A. A. Barbosa, P. Brequigny, F. Contino, C. Mounaïm-Rousselle, L. Seidel, F. Mauss, An experimental and modeling study of ammonia with enriched oxygen content and ammonia/hydrogen laminar flame speed at elevated pressure and temperature, Proc. Combust. Inst. (2020) 2163–2174.

[19] F. Halter, Z. Chen, G. Dayma, C. Bariki, Y. Wang, P. Dagaut, C. Chauveau, Development of an optically accessible apparatus to characterize the evolution of spherically expanding flames under constant volume conditions, Combust. Flame 212 (2020) 165–176.

[20] F. Halter, G. Dayma, Z. Serinyel, P. Dagaut, C. Chauveau, Laminar flame speed determination at high pressure and temperature conditions for kinetic schemes assessment, Proc. Combust. Inst. 38 (2021) 2449–2457.

[21] R. R. Burrell, J. L. Pagliaro, G. T. Linteris, Effects of stretch and thermal radiation on difluoromethane/air burning velocity measurements in constant volume spherically expanding flames, Proc. Combust. Inst. 37 (2019) 4231–4238.

[22] K. Eisazadeh-Far, A. Moghaddas, H. Metghalchi, J. C. Keck, The effect of diluent on flame structure and laminar burning speeds of JP-8/oxidizer/diluent premixed flames, Fuel 90 (2011) 1476–1486.

[23] M. Faghih, Z. Chen, The constant-volume propagating spherical flame method for laminar flame speed measurement, Sci. 61 (2016) 1296–1310.

[24] C. Xiouris, T. Ye, J. Jayachandran, F. N. Egolfopoulos, Laminar flame speeds under engine-relevant conditions: Uncertainty quantification and minimization in spherically expanding flame experiments, Combust. Flame 163 (2016) 270–283.

[25] S. J. Klippenstein, M. Pfeifle, A. W. Jasper, P. Glarborg, Theory and modeling of relevance to prompt-NO formation at high pressure, Combust. Flame 195 (2018) 3–17.

[26] P. Dagaut, P. Glarborg, M. Alzueta, The oxidation of hydrogen cyanide and related chemistry, Prog. Energy Combust. Sci. 34 (2008) 1–46.

[27] Y. Zhang, O. Mathieu, E. L. Petersen, G. Bourque, H. J. Curran, Assessing the predictions of a NO_x kinetic mechanism on recent hydrogen and syngas experimental data, Combust. Flame 182 (2017) 122–141.

[28] K. P. Shrestha, L. Seidel, T. Zeuch, F. Mauss, Detailed kinetic mechanism for the oxidation of ammonia including the formation and reduction of nitrogen oxides, Energy Fuels 32 (2018) 10202–10217.

[29] H. Nakamura, S. Hasegawa, Combustion and ignition characteristics of ammonia/air mixtures in a micro flow reactor with a controlled temperature profile, Proc. Combust. Inst. 36 (2017) 4217–4226.

[30] E. C. Okafor, Y. Naito, S. Colson, A. Ichikawa, T. Kudo, A. Hayakawa, H. Kobayashi, Measurement and modelling of the laminar burning velocity of methane-ammonia-air flames at high pressures using a reduced reaction mechanism, Combust. Flame 204 (2019) 162–175.

[31] J. Otomo, M. Koshi, T. Mitsumori, H. Iwasaki, K. Yamada, Chemical kinetic modeling of ammonia oxidation with improved reaction mechanism for ammonia/air and ammonia/hydrogen/air combustion, Int. J. Hydrog. Energy 43 (2018) 3004–3014.

[32] A. Stagni, C. Cavallotti, S. Arunthanayothin, Y. Song, O. Herbinet, F. Battin-Leclerc, T. Faravelli, An experimental, theoretical and kinetic-modeling study of the gas-phase oxidation of ammonia, React. Chem. Eng. 5 (2020) 696–711.

[33] O. Mathieu, E. L. Petersen, Experimental and modeling study on the high-temperature oxidation of ammonia and related NO_x chemistry, Combust. Flame 162 (2015) 554–570.

[34] R. C. da Rocha, M. Costa, X.-S. Bai, Chemical kinetic modelling of ammonia/hydrogen/air ignition, premixed flame propagation and NO emission, Fuel 246 (2019) 24–33.

[35] D. Wang, C. Ji, Z. Wang, S. Wang, T. Zhang, J. Yang, Measurement of oxy-ammonia laminar burning velocity at normal and elevated temperatures, Fuel 279 (2020) 118425.

[36] A. Konnov, Implementation of the NCN pathway of prompt-NO formation in the detailed reaction mechanism, Combust. Flame 156 (2009) 2093–2105.

[37] A. A. Konnov, A. Mohammad, V. R. Kishore, N. I. Kim, C. Prathap, S. Kumar, A comprehensive review of measurements and data analysis of laminar burning velocities for various fuel+air mixtures, Prog. Energy Combust. Sci. 68 (2018) 197–267.